Anal. Chem. **2006,** *78,* 3444−3451

Electron Multiplying Charge-Coupled Device Camera Based Fluorescence Correlation Spectroscopy

Balakrishnan Kannan,[†] Jia Yi Har,[†,‡,§] Ping Liu,[†,||] Ichiro Maruyama,[||] Jeak Ling Ding,[‡,§] and Thorsten Wohland*[,†,§]

Department of Chemistry, 3, Science Drive 3, and Department of Biological Sciences, 14, Science Drive 4, National University of Singapore, Singapore 117543, Singapore—MIT Alliance, E4-04-10, 4, Engineering Drive 3, Singapore 117576, and Genome Institute of Singapore, 60, Biopolis Street, Singapore 138672

A fluorescence correlation spectroscopy (FCS) setup is built with an electron multiplying charge-coupled device camera. Although the instrument has a limited time resolution of 4 ms, compared to 0.1−0.2 μs for common instruments using avalanche photodiodes, it allows multiplexing of FCS measurements, has a software-adjustable pinhole after data collection, performs flow speed as well as flow direction measurements in microchannels and could be used to do spectral FCS. Measurements are performed on fluorescent dyes and polystyrene beads in high-viscosity media and on epidermal growth factor receptors in Chinese hamster ovary cells. Using real measurements on single spots, multiplexing of focal spots and detection elements are simulated and the results are discussed.

Fluorescence correlation and cross-correlation spectroscopy (FCS, FCCS) are widely used tools to study molecular dynamics from diffusion coefficients, molecular interactions, flow rates to membrane dynamics, and several reviews have been published recently.[1−3] Present systems use either avalanche photodiodes (APD) or photomultipliers as detectors, allowing usually only measurement with up to four detectors.[4] Recently, a system using diffractive optical elements was used to create up to four different spots detected by a 2 × 2 CMOS detector array[5] or an array of APDs.[6] A different approach to study dynamics with temporal and spatial resolution is image correlation spectroscopy[7] (ICS). Recently, an extension of ICS, raster image correlation spectroscopy[8] (RICS), was introduced. RICS exploits the hidden time structure of a scanned confocal image and was used[8] to extract diffusion times of membrane proteins in live cells. However, for many experiments, it would be important to perform FCS measurements simultaneously on a large number of spots, e.g., on cell membranes or for flow speed and flow direction measurements, to lower the overall measurements time, as well as allowing the simultaneous determination of parameters in a whole system, instead of a sequential acquisition during which the parameter could undergo significant changes.

In this article, a new method to perform FCS using an electron multiplying charge-coupled device (EMCCD) camera is described. Experiments are done with a single focal volume for calibration of the performance of the device and determination of minimum distance between adjacent focal volumes necessary for multiplexing. Despite the low temporal resolution (4 ms), it is shown that the diffusion of the epidermal growth factor receptor (EGFR) labeled with a monomeric red fluorescent protein (mRFP) can be measured in Chinese hamster ovary (CHO) cells, and flow directions in microchannels can be determined by cross-correlation of different pixel elements surrounding the focal spot.

EXPERIMENTAL DETAILS

The EMCCD camera based FCS system has been built around an inverted epifluorescence microscope (Axiovert 200M, Carl Zeiss, Singapore). Laser light from a 543-nm He−Ne laser (Melles Griot, Singapore) was beam-expanded three times and focused at the conjugate image plane on the illumination port of the microscope. A dichroic mirror (560DRLP, Omega, Brattleboro, VT) reflected the incident laser light into a water immersion objective (60×, NA 1.2, Olympus, Singapore). The excitation laser power as measured before the objective was 100 μW for Atto565 (static and flow measurements) and 60 μW for fluospheres and CHO cells. The emitted fluorescence light from the fluorophores within the focal volume was collected by the same objective and passed through the dichroic mirror and the emission filter (595AF60, Omega, Brattleboro, VT) before being collected by the EMCCD camera (Cascade: 512B, Photometrics, Tucson, AZ)

* Corresponding author. E-mail: chmwt@nus.edu.sg. Fax: +65-6779 1691.
† Department of Chemistry, National University of Singapore.
‡ Department of Biological Sciences, National University of Singapore.
§ Singapore—MIT Alliance.
|| Genome Institute of Singapore.

(1) Krichevsky, O.; Bonnet, G. *Rep. Prog. Phys.* **2002**, *65*, 251−297.
(2) Thompson, N. L.; Lieto, A. M.; Allen, N. W. *Curr. Opin. Struct. Biol.* **2002**, *12*, 251−297.
(3) Gösch, M.; Rigler, R. *Adv. Drug Delivery Rev.* **2005**, *57*, 169−190.
(4) (a) Heinze, K. G.; Jahnz, M.; Schwille, P. *Biophys. J.* **2004**, *86*, 506−516. (b) Burkhardt, M.; Heinze, K. G.; Schwille, P. *Opt. Lett.* **2005**, *30*, 2266−2268.
(5) Gösch, M.; Serov, A.; Anhut, T.; Lasser T.; Rochas, A.; Besse, P. A.; Popovic, R. S.; Blom, H.; Rigler, R. *J. Biomed. Opt.* **2004**, *9*, 913−921.
(6) Gösch, M.; Blom, H.; Anderegg, S.; Korn, K.; Thyberg, P.; Wells, M.; Lasser, T.; Rigler, R.; Hard, A. M. S. *J. Biomed. Opt.* **2005**, *10*, 054008.
(7) Petersen, N. O.; Höddelius, P. L.; Wiseman, P. W.; Seger, O.; Magnusson, K. E. *Biophys. J.* **1993**, *65*, 1135−1146.
(8) Digman, M. A.; Brown, C. M.; Sengupta, P.; Wiseman, P. W.; Horwitz, A. R.; Gratton, E. *Biophys. J.* **2005**, *89*, 1317−1327.

10.1021/ac0600959 CCC: $33.50
Published on Web 04/19/2006

mounted on the base port of the microscope. The camera and microscope were controlled by the Metamorph software (Universal Imaging Corp., Downingtown, PA). The back-illuminated EMCCD sensor has more than 90% quantum efficiency in the wavelength range from 500 to 650 nm and is a frame-transfer device. The image section of the frame-transfer device has a physical dimension of 8.2×8.2 mm^2, which is divided into 512×512 pixels yielding 16×16 μm^2/pixel. When operated in overlap mode, the time resolution is limited by the frame read time (FRT), which consists of serial clear time, parallel (vertical) shift time, serial discard time, and serial conversion time. Among these, the serial clear time and the serial discard time are smaller when compared to the parallel (vertical) shift time [= 2 μs/row $\times$ 524 rows (512 rows in image section + 12 dark reference (dummy) rows) = 1.048 ms] and the serial conversion time (= 100 ns/pixel with 10-MHz digitizer). The frame acquisition time (FAT) is a sum of clear count $\times$ parallel clear time, shutter (open + close) delay, exposure time, and parallel (vertical) shift time. In the "stream acquisition", if "clear presequence" and "open shutter presequence" options are chosen, then the first two contributions to FAT are zero. The parallel (vertical) shift time in FAT is the same (1.048 ms) as that in FRT. So, the exposure time is FAT $-$ 1.048 ms. For this camera, FRT is 33.9 ms for a 512×512 region of interest (ROI) and 6.47 ms for a 64×64 ROI, without binning. However, the time resolution can be improved by having a smaller ROI. The best time resolution found with this camera is 4 ms for a ROI of 20×20 or a smaller square array (without or with binning) and 1×170 rectangular array (without or with binning). When the FAT is set to 4 ms for a ROI, say 20×20 without binning, the actual exposure time is $4 - 1.048 = 2.952$ ms.

The EMCCD camera allows binning of pixels (so-called "hardware binning") where a number of pixels are combined into one "binned" pixel. A hardware-binned frame can be acquired and then the photon counts of each binned pixel can be logged out from the frame. Alternately, a frame with no binning can be acquired and then the photon counts of all the pixels in a chosen array of $m \times n$ can be summed (so-called "software binning") to get photon counts of the $m \times n$ binned pixels. Both the hardware binning and the software-binning yield the same results as long as the background is subtracted (see below). The advantage with the software binning is that arrays of different sizes can be chosen for the particular experimental consideration any time after the data collection. In this work, only symmetrical binning (hardware binning or software binning) was used to create binned pixels of $n \times n$ pixel size. Pixels are denoted according to their size by P_n to denote $n \times n$ binned pixels. P_3 pixels were used in all the measurements except in the experiments investigating the effect of binning and flow direction measurements. The actual distance s in the sample (μm) for a given pixel distance d and pixel P_n can be calculated by $s = (d \times n \times 16)/54.7$ μm. The magnification of a factor 54.7 results from the usage of a 60$\times$ Olympus objective on a Zeiss microscope, since the two manufacturers use different tube length thus leading to small deviations in the magnification.

A ROI with 20×20 pixels with either P_1 or P_3 was created that encompasses the image of the focused laser beam at the center. A stack of 10 000 frames of the ROI was acquired with a 4-ms FAT with the intensifier gain fixed at 75% of the maximum and read using a 10-MHz digitizer. Photon counts at each pixel within the ROI along with the time stamps were logged out from the 10 000 frames using Metamorph software. The photon counts thus extracted contain the background counts, which are a sum of the electronic offset of the A/D converter in the camera (dependent on each individual camera and manufacturer), the autofluorescence, and the leakage of the excitation laser intensity into the CCD. To find out the background counts, the negative control [mixture of glycerol and phosphate-buffered saline (PBS) in the same ratio as in the fluorescent samples or the PBS alone] was measured under identical experimental conditions. The minimum found from the photon counts of all the pixels within the ROI in the stack is taken as the offset, and it was subtracted from the photon counts of all the pixels in the stack acquired on the fluorescent samples. Autocorrelation functions, $G(\tau)$, and cross-correlation functions, $G_x(\tau)$, were calculated from the photon counts (software binned or hardware binned) using the algorithm given in ref 9.[9]

For comparison, correlation curves of all the solutions used in this work were measured in an FCS instrument, which was built around a confocal laser scanning microscope (LSM; FV300, Olympus). The detection part for FCS was mounted on top of the scanning unit of the LSM. The fluorescence light that passed the confocal pinhole (50 μm) was imaged by a lens (Achromat $f = 60$ mm, Linos, Göttingen, Germany) through an emission filter into the active area of the APD in a single photon counting module (SPCM-AQR-14, Pacer Components, Berkshire, UK). The TTL output signal from the SPCM is processed online by an autocorrelator (Flex02-01D, correlator.com, Zhejianj, China) to get an experimental autocorrelation curve, $G(\tau)$. The excitation wavelength, dichroic mirror, emission filter, and objective were the same as in the EMCCD system.

The fluorophores used in the experiments were (i) Atto565 (Sigma-Aldrich, Singapore, $\lambda_{ex} = 563$ nm, $\lambda_{em} = 592$ nm) and (ii) Fluospheres (Invitrogen, F-8786, radius 0.01 μm, $\lambda_{ex} = 580$ nm, $\lambda_{em} = 605$ nm). Atto565 in PBS was mixed with glycerol (in v/v ratio) to obtain 1, 2, 4, and 8 nM concentrations in 90% glycerol or 1 nM in 80% glycerol solutions. Fluospheres in the stock solution were diluted 15 times with deionized water and then mixed with glycerol to yield solutions with 80 and 90% glycerol content.

Cell Preparation. The EGFR-mRFP construct was made by attaching the mRFP to the carboxyl terminus of the human EGFR by standard recombinant techniques. Plasmid DNA was prepared by using EndoFree Plasmid Maxi Kit (Qiagen GmbH). CHO-K1 cells (ATCC, Manassas, VA) were grown to 70% confluency in Ham's F-12K medium (with Kaighn's modification) supplemented with 2 mM L-glutamine, 1.5 g/L sodium bicarbonate, 50 units/mL penicillin G, and 50 μg/mL streptomycin and supplemented with 10% fetal bovine serum at 37 °C in 5% (v/v) CO_2 humidified atmosphere in T75 culture flasks. Cells were then washed with PBS and trypsinized. For each reaction, $3-5 \times 10^6$ cells were mixed with 5 μg of plasmid in 200 μL of normal growth medium in a 0.2-cm cuvette (Bio-Rad, Hercules, CA) and electroporated by the Gene Pulser (Bio-Rad) using the preset experimental parameters. Transfected cells were seeded on 30-mm-diameter circular coverslips in six-well plate and grown in culture medium for 2 days. To inhibit endocytosis, cells were starved with reduced-

(9) Wohland, T.; Rigler, R.; Vogel, H. *Biophys. J.* **2001**, *76*, 2987−2999.

serum medium (0.2% serum in F-12K) for 4−8 h before measurements. During the FCS measurements, the circular coverslips were washed with PBS, mounted on a sample well, and filled with PBS.

Microchannel. Flow measurements were carried out in a microchannel with a rectangular cross section of 380-μm width and 300-μm height. Teflon was used to fabricate a microchannel mold with one inlet and two outlets. Prepolymer of poly(dimethylsiloxane) (PDMS) (Sylgard 184, Dow-Corning, Midland, MI) was poured over the molds and cured at 65 °C overnight before peeling off. The PDMS membrane was oxidized in oxygen plasma for 1 min in order to chemically bond to a glass coverslip. A syringe pump (NE-1000, New Era Pump Systems Inc., Farmingdale, NY) was employed for the perfusion of probe solution into the microchannels through tubing and connectors. Different flow velocities in the microchannel can be induced by varying the pumping rates.

FCS Data Analysis. The autocorrelation curves of dye solutions were fitted to an equation describing the Brownian motion of the fluorophores in a three-dimensional Gaussian volume element.

$$G(\tau) = \frac{1}{N}\left(1 + \frac{\tau}{\tau_D}\right)^{-1}\left(1 + \frac{\tau}{K^2\tau_D}\right)^{-0.5} + G_\infty \qquad (1)$$

where τ_D is the diffusion time of the fluorophores within the focal volume, given by $\tau_D = \omega_0^2/4D$, D being the diffusion coefficient of the fluorophore. The structure factor $K = z_0/\omega_0$ takes into account the asymmetry of the focal volume, where z_0 and ω_0 are the axial and radial distances, respectively, at which the excitation intensity reaches $1/e^2$ of its value at the center of the focal volume. N is the number of molecules within the focal volume. The additive constant G_∞ is the convergence value of $G(\tau)$ for long times and was close to 1 in all cases as expected.

The diffusion of EGFR along the cell membrane of CHO cells is a two-dimensional (2D) phenomenon and hence the $G(\tau)$ of CHO cells were fitted to 2D diffusion model given by

$$G(\tau) = \frac{1}{N}\left(1 + \frac{\tau}{\tau_D}\right)^{-1} + G_\infty \qquad (2)$$

For the determination of flow speed, the flow data were fitted to the flow model[10]

$$G_F(\tau) = \frac{1}{N} g(\tau)\, \exp\left[-\left(\frac{\tau}{\tau_F}\right)^2 g(\tau)\right] + G_\infty \qquad (3)$$

where $g(\tau) = (1 + \tau/\tau_D)^{-1}(1 + \tau/K^2\tau_D)^{-0.5}$ and τ_F is the flow time within the focal volume. Calculation of correlation curves from the intensity data and fitting of correlation curves were carried out using self-written programs in IGOR Pro (Wavemetrics, Lake Oswego, OR).

RESULTS AND DISCUSSION

Calibration. For the calibration of the system, the dependence of $G(\tau)$ on concentration, particle size, and viscosity was tested (Figure 1, Table 1). The average diffusion time of Atto565 in 90% glycerol (Figure 1, upper panel) was $\tau_D = 40.0 \pm 15.3$ ms with the focal volume defined by a P_3 pixel, corresponding to a 48 × 48 μm^2 pinhole, with the laser focus at the center. No correlation was found in the negative control. For comparison, the same solutions were measured in a standard FCS instrument and fitted to eq 1 (Table 1). The number of particles seen on the EMCCD setup is a factor of ~2 higher for all cases and τ_D is a factor of 2−3 larger for the EMCCD setup. The difference in the value of τ_D obtained from the two systems can be explained by the fact that (i) the difference in coupling of the laser beam into the microscope for the EMCCD and the standard FCS systems, (ii) the difference in the magnification (54.7× for the EMCCD-FCS system, 60× for the standard FCS system) arising out of using the same 60 × Olympus objective in the two systems (see the Experimental Details), and (iii) the difference in pinhole (48 × 48 μm^2 square pinhole in the EMCCD system and 50-μm-diameter circular pinhole in the standard FCS system) and hence the focal volumes are different in the two systems. The difference in the focal volumes can be seen in the difference in the beam waist (ω_0) for the two systems when measuring the samples in glycerol. The calculated ω_0 value by using the values of τ_D (Table 1) and D (1.3×10^{-12} m^2/s) of Atto565 samples in 90% glycerol for the standard FCS setup is 0.28 ± 0.01 μm and the EMCCD-FCS setup is 0.46 ± 0.02 μm. This manifests as well in the values of the structure factor K (eq 1), which is 3.0 ± 1.1 in the EMCCD setup compared to 5.05 ± 0.34 in the standard FCS setup. The ω_0 values thus determined are somewhat larger than expected due to the mismatch in refractive index between water as immersion medium and glycerol/water mixtures as mounting medium. For the standard FCS setup, the ω_0 value in deionized water is 0.22 ± 0.02 μm. Nevertheless, for both setups, the amplitude of $G(\tau)$ decreased and the particle number N increased with concentration as expected by a factor of ~2 for each doubling of the concentration (Table 1). The standard deviation of τ_D for all measurements is larger for the EMCCD setup, which is a result of its much lower time resolution. With increasing particle size (Atto565 compared to fluospheres) or viscosity (80−90% glycerol), τ_D increased as

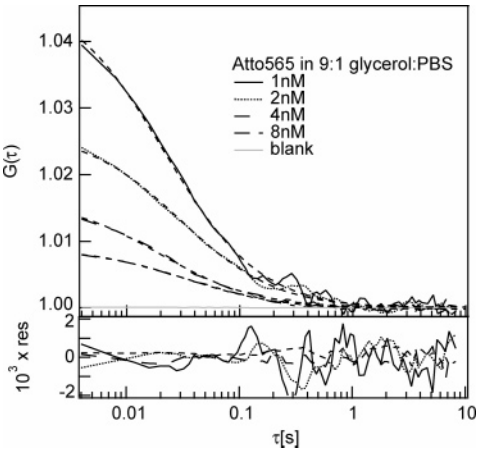

Figure 1. Dependence of the autocorrelation function, $G(\tau)$, on concentration. Measurements were taken with 1, 2, 4, and 8 nM Atto565 in a 9:1 glycerol/PBS mixture. All measurements were done at 100 μW at a wavelength of 543 nm using a P_3 pixel (software binned) of the CCD. The upper panel shows the $G(\tau)$ and the accompanying fits (eq 1). The lower panel shows the fit residuals.

(10) (a) Magde, D.; Webb, W. W.; Elson, E. L. *Biopolymers.* **1978**, *17*, 361−376. (b) Gösch, M.; Blom, H.; Holm, J.; Heino, T.; Rigler, R. *Anal. Chem.* **2000**, *72*, 3260−3265.

Table 1. Particle Number *N* and Diffusion Time τ_D Obtained by Fitting the $G(\tau)$ Curves, Measured on Different Concentrations of Atto565 and 15× Diluted Fluospheres in Aqueous Solutions of Glycerol with Different Glycerol Content (% G) Using the Standard FCS and the EMCCD-FCS with P_3 Pixel, to Eq 1

sample/concn/glycerol content (%)	EMCCD-FCS		standard FCS	
	N	τ_D (ms)	N	τ_D (ms)
Atto565, 8 nM, 90	121.0 ± 11.4	45.5 ± 8.5	66.8 ± 2.9	14.3 ± 1.6
Atto565, 4 nM, 90	69.3 ± 6.6	38.3 ± 12.9	33.3 ± 2.5	15.4 ± 2.7
Atto565, 2 nM, 90	37.8 ± 0.9	36.2 ± 4.8	19.0 ± 0.9	15.4 ± 1.8
Atto565, 1 nM, 90	22.4 ± 1.6	40.0 ± 15.3	9.5 ± 1.1	14.2 ± 0.8
Atto565, 1 nM, 80	10.0 ± 6.7	10.8 ± 1.1	5.0 ± 1.5	5.1 ± 0.3
fluospheres, 15× , 90	3.4 ± 1.1	770.2 ± 249.7	3.1 ± 0.3	352.7 ± 11.7
fluospheres, 15× , 80	5.8 ± 0.4	285.5 ± 119.3	4.2 ± 2.5	125.5 ± 25.0

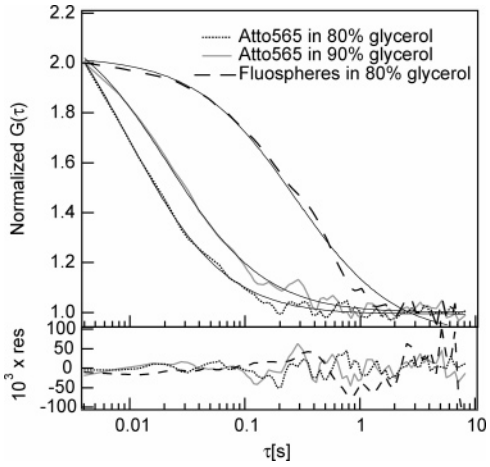

Figure 2. Dependence of the autocorrelation function, $G(\tau)$, on viscosity and particle size. The normalized $G(\tau)$ of Atto565 in two solutions of different viscosities (glycerol/PBS mixtures of 8:2 and 9:1), and of fluorescent polystyrene beads (0.01-μm radius) in a glycerol/PBS mixtures of 8:2 are shown. Measurements on Atto565 were performed with 100-μW laser power and the measurements on beads with 60-μW laser power at a wavelength of 543 nm using a P_3 pixel (software binned) of the CCD. The upper panel shows the normalized $G(\tau)$ and the accompanying fits (eq 1). The lower panel shows the fit residuals.

shown in Figure 2. The fitted values of N and τ_D and the comparison with the standard FCS setup is given in Table 1. Again, the measured τ_D of the EMCCD setup is greater by a factor of 2−3 than for the standard FCS setup, but all the ratios of the diffusion times for different measurements are similar in all cases for each setup. From the Stokes−Einstein equation ($D = k_BT/6\pi\eta r_h$, k_B the Boltzmann constant, T the absolute temperature, η the viscosity of the solution, and r_h the hydrodynamic radius of the molecule), it is known that $D_1/D_2 = \eta_2/\eta_1 = \tau_2/\tau_1$. The calculated ratios ($\tau_{90\%G}/\tau_{80\%G}$) from the diffusion times of Atto565 in 90 and 80% glycerol for the two systems (2.91 for the standard FCS system and 3.7 for the EMCCD-FCS system) are close to the ratio ($\eta_{90\%G}/\eta_{80\%G} = 3.37$) of viscosities of aqueous solutions of glycerol[11] at 25 °C.

Binning. The choice of P_3 corresponds to a square pinhole with dimensions of 48 × 48 μm^2. Adapting the pinhole to the correct size is important in FCS,[12] and changes in pinhole size can be useful to determine whether a particular process is diffusion dependent[13] or whether anomalous diffusion is present.[14] We thus used software binning to change the pinhole size to P_1, P_3, P_5, and P_7 pixels (16−112-μm side length) for the case of 1 nM Atto565 in 90% glycerol (Figure 3a, Table 2). Both N and τ_D increased with binning as expected since a larger volume is detected with an increasing pinhole size. Similarly, the structure factor K increased with increasing binning until for the P_7 pixels, the fits did not converge anymore when K is kept free since the pinhole is not performing its spatial filtering function anymore when it becomes too large. These measurements demonstrate the capability of this system to change the pinhole size after data collection.

Multiplexing. For multiplexing, the "cross talk" of the fluorescence intensity originating from one focal volume into the detection elements corresponding to the neighboring focal volumes has to be minimized. To characterize this separation, $G(\tau)$ of two P_3 pixels (hardware binned) with variable distance along a whole line of the CCD (1 × 170 P_3) were calculated. The laser was focused on 95th P_3 pixel allowing measurements of up to a distance of 95 P_3 pixels. The fluorescence intensity and $G(\tau)$ amplitudes, normalized to the center element, decrease with increasing distance of the P_3 pixel from the focal spot (Figure 3b). While the intensity decreases slower, the $G(\tau)$ amplitude decreases faster and no correlation can be detected anymore at a distance of more than about 5−10 P_3 pixels. Figure 3c shows normalized $G(\tau)$ of the central P_3 pixel and pixels at a distance of 10 P_3 pixels to the left and right of the focal spot. The actual distance at which no correlation can be seen anymore depends on the absolute amount of cross talk and thus on the brightness of the particle under investigation. To be conservative, we assumed for all multiplexing cases a distance of 10 P_3 pixels between focal volumes. This indicates that, in principle, it is possible to have an array of 17 × 17 detection elements, each consisting of a P_3 pixel and, hence, 289 focal volumes with this CCD. However, it must be borne in mind that the time resolution will be ~13 ms only in this case. It should be noted that newer camera models on the market with less number of pixels (128 × 128) and higher readout rates (12-MHz digitizer) offer time resolutions down to 1 ms.

To further characterize the influence of focal spots on each other in a multiplexing experiment, multifocal spot experiments

(11) (a) Segur, J. B.; Oberster, H. E. *Ind. Eng. Chem.* **1951**, *43*, 2117. (b) Sheeley, M. L. *Ind. Eng. Chem.* **1932**, *24*, 1060.
(12) (a) Rigler, R.; Mets, Ü.; Widengren, J.; Kask, P. *Eur. Biophys. J.* **1993**, *22*, 169−175. (b) Hess, S. T.; Webb, W. W. *Biophys. J.* **2002**, *83*, 2300−2317.
(13) Widengren, J.; Mets, Ü.; Rigler, R. *Chem. Phys.* **1999**, *250*, 171−186.
(14) (a) Weiss, M.; Hashimoto, H.; Nilsson, T. *Biophys. J.* **2003**, *84*, 4043−4052. (b) Wawrezinieck, L.; Rigneault, H.; Marguet, D.; Lenne, P. F. *Biophys. J.* **2005**, *89*, 4029−4042. (c) Masuda, A.; Ushida, K.; Okamoto, T. *Biophys. J.* **2005**, *88*, 3584−3591.

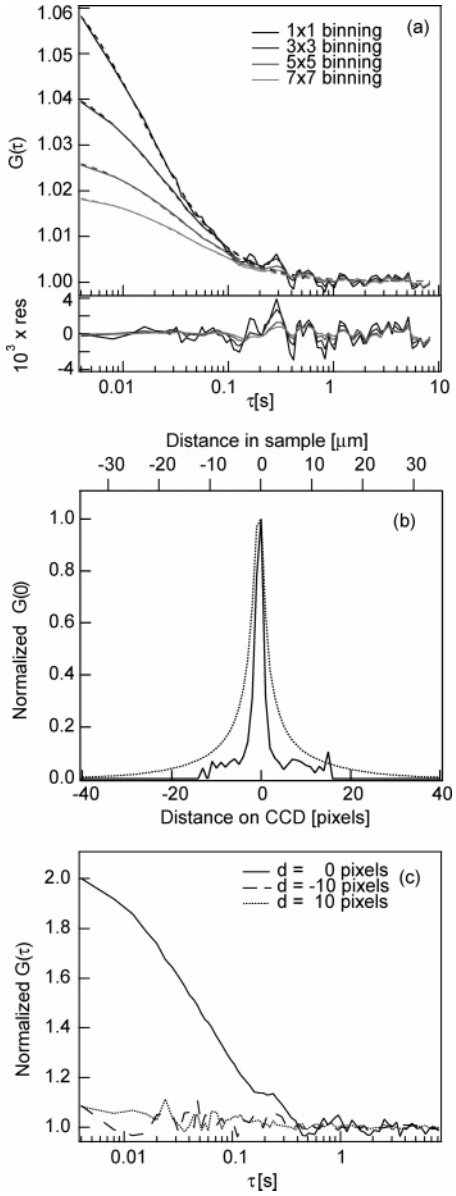

Figure 3. (a) Influence of binning on the autocorrelation function, $G(\tau)$. Increasing the software-binned area from P_1 up to P_7 leads to a decrease in the amplitude of the $G(\tau)$ and an increase in τ_D (see Table 2). The upper panel shows the $G(\tau)$ and the accompanying fits (eq 1). The lower panel shows the fit residuals. (b) Intensity (dotted line) and $G(\tau)$ amplitude (solid line) measured in P_3 pixels (hardware binned) along a line of the CCD. The central P_3 pixel coincides with the center of the focal volume. Intensity and $G(\tau)$ amplitude decrease with increasing distance of the P_3 pixel from the focal spot. While the intensity decreases slower, the $G(\tau)$ amplitude decreases faster and vanishes at a distance of more than 10 P_3 pixels. (c) Normalized $G(\tau)$ of central P_3 pixel (hardware binned) and pixels at a distance of 10 P_3 pixels to left and right of the focal spot. All measurements were done at 100 μW at a wavelength of 543 nm.

are simulated. For this purpose, autocorrelation curves of individual focal spots with P_3 pixels (hardware binned) are taken. The individual frames in time of n such measurements are then shifted with respect to each other by 10 P_3 pixels in x or y direction and added by software. This procedure results in one stack of frames where each frame contains the fluorescence information of all n focal spots and the cross talk into all neighboring pixels. Although this is not a real multiplexing experiment, it is a good estimation since fluorescence is a linear process and the fluorescence from each P_3 pixel is the addition of the fluorescence stemming from all n focal spots. One should note that real experiments are limited by the dynamic range of the CCD, and one should take care not to saturate the pixels since otherwise information will be lost and results will be biased. Nevertheless, this procedure allows the evaluation in how far multiplexing is at all possible with this setup.

Table 2. Particle Number N and Diffusion Time τ_D Obtained by Fitting the $G(\tau)$ Curves, Measured on 1 nM Atto565 in Aqueous Solutions of Glycerol with 90% Glycerol Content with Different Binning Using the EMCCD-FCS, to Eq 1

	EMCCD-FCS	
binning	N	τ_D [ms]
1× 1	15.6 ± 3.1	26.8 ± 11.0
3× 3	22.4 ± 1.6	40.0 ± 15.3
5× 5	33.7 ± 0.9	56.7 ± 22.4
7× 7	47.2 ± 2.8	71.4 ± 28.3

Figure 4a shows the change of the amplitude $G(0)$ when two focal spots are measuring Atto565 (90% glycerol) in dependence of the separation of the two spots. The results are normalized to the autocorrelation amplitude expected for an individual, isolated focal spot. It can be seen that only at large distances of 60 P_3 pixels does the amplitude converge to its normal value. This is a result of the much slower decrease of intensity cross talk into neighboring P_3 pixels compared to actual correlations (Figure 3b). While at a distance of 10 P_3 pixels no appreciable correlations can be detected anymore (Figure 3b), intensity cross talk is still high enough to influence the amplitude of correlation functions (Figure 4a). In this case, the cross talk contributes mainly as an uncorrelated background signal to the measurement. This is further corroborated by the results of Figure 4b where two focal spots (P_3 pixels), one measuring Atto565 (90% glycerol) the other fluospheres, are overlaid. The plot shows τ_D of the two focal spots in dependence of their separation. At a distance of 0 P_3 pixels, i.e., complete overlap of the two focal spots, the τ_Ds are exactly the same and lie between the expected τ_D for Atto565 and the fluospheres. For increasing separation of the two focal spots, the τ_Ds converge to their expected values for Atto565 and the fluospheres. And at a separation of more than 5−10 P_3 pixels, there is no influence detectable anymore on the τ_D values of the different focal spots. Selected $G(\tau)$ curves for the focal spot measuring Atto565 are shown in Figure 4c to demonstrate the progression from complete overlap, where the curve is strongly influenced by the fluosphere signal, to the situation at wide separation, where the influence of the fluospheres is negligible due to the minimal cross talk.

To show the feasibility of measurements with more focal spots, a simulation of 9 focal spots on a grid with a distance of 10 P_3 pixels in x and y directions, where all focal spots measure an Atto565 solution (90% glycerol), was made. Figure 4d shows the amplitudes of the $G(\tau)$ curves as a fraction of the expected amplitudes. Clearly the central spot, which sees the largest amount of cross talk from neighboring spots, has the lowest amplitude, while the corner spots with the least number of neighboring spots

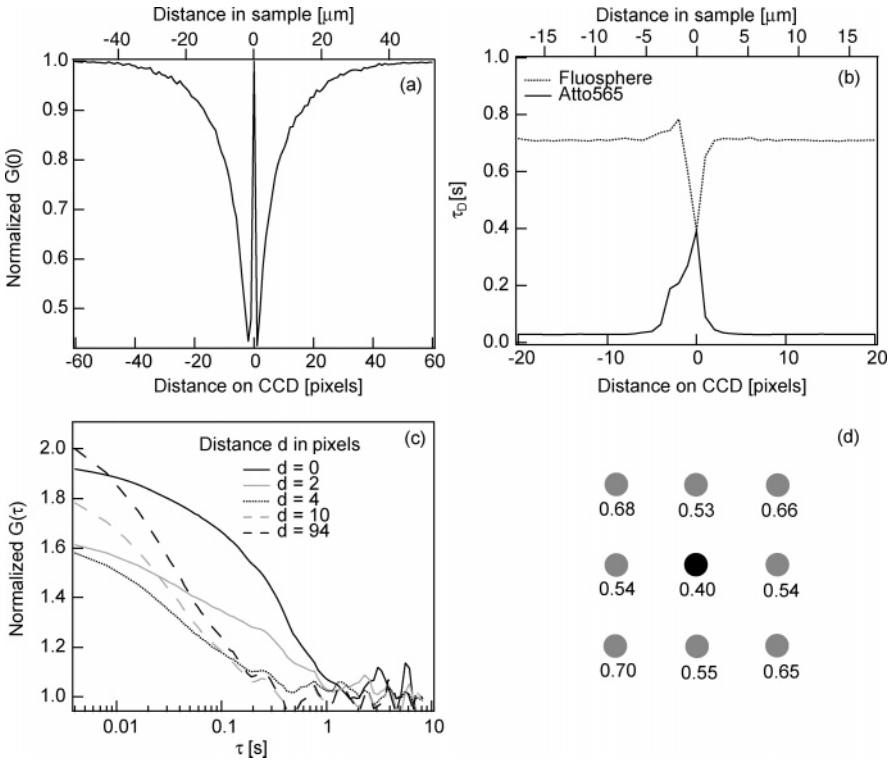

Figure 4. Possibility of multiplexing assuming P_3 binning. All data are simulated using real independent measurements of single spots as described in the text with P_3 (hardware) binning. (a) Autocorrelation function amplitude $G(0)$ of one focal spot in dependence of the position of a second focal spot. Both spots measure the same sample, and thus no influence on τ_D is expected. In the center at position 0, the two focal spots overlap. In this case, the count rate per particle would increase (neglecting saturation effects) but the amplitude would stay constant. When there is a distance between the two spots, the cross talk of the second spot to the first will influence the amplitude of the $G(\tau)$. The larger the distance, the less important will be the cross talk and the amplitude of the $G(\tau)$ will converge to its original value. (b) Diffusion time τ_D in dependence of the distance of two focal spots (P_3 pixels) which measure two different samples (Atto565, fluospheres). When the two focal spots (P_3 pixels) overlap the diffusion coefficient of spot 1 (Atto565, solid line) and spot 2 (fluospheres, dotted line) are equal since this situation represents a mix of two samples measured in the same focal spot. If the spots are separated, corresponding to two spots measuring simultaneously two different samples, the cross talk between the focal spots will lead to diffusion times that are a weighted average of the two spots. However, it can be seen that already at a separation of 5 P_3 pixels the diffusion times have converged to their actual value and cross talk is negligible. (c) Examples of the $G(\tau)$ of example b at different separations. (d) Amplitude of $G(\tau)$ if 9 focal spots all measuring Ato565 in 9:1 glycerol/PBS mixture ordered in a square with distances of 10 P_3 pixels horizontally and vertically. At this distance, there should be only an influence on the amplitude but not on the diffusion time τ_D. The numbers give the fraction of the amplitude compared to a single spot.

and thus the smallest amount of cross talk have the largest amplitudes.

To determine the influence of the neighboring spots on the correlation time, we investigated the case where the central spot (P_3 pixel) is measuring an Atto565 solution (90% glycerol) and the eight surrounding focal spots (P_3 pixels) measure fluosphere solutions. The measured τ_D is 23.7 ± 5.6 ms for the central spot in the absence of the other spots and 22.5 ± 5.6 ms in the presence of all spots. Within the errors of these measurements, these values are the same and the experiment confirms that, while the amplitude of the $G(\tau)$ curves is influenced over wider distances, a distance of 10 P_3 pixels is enough to ensure that there is no influence on the characteristic time of the $G(\tau)$.

Cell Measurements. Next, the suitability of the system for biological applications was tested by measuring the diffusion time of mRFP-labeled EGFR in CHO cells using a P_3 pixel (software binned) of the CCD. A representative $G(\tau)$ curve measured on the upper membrane of a CHO cell is shown in Figure 5 along with the negative control measured in PBS between two adjacent cells. Data were fitted to eq 2 and the values of τ_D obtained range from 10 to 140 ms. This is comparable to the values of $\tau_D = 54 \pm 27$ ms (with extreme values of 11 and 159 ms, measured on 408 different cells) obtained on mRFP-labeled EGFR in CHO cells[15] prepared under a protocol identical to that for the cells used in

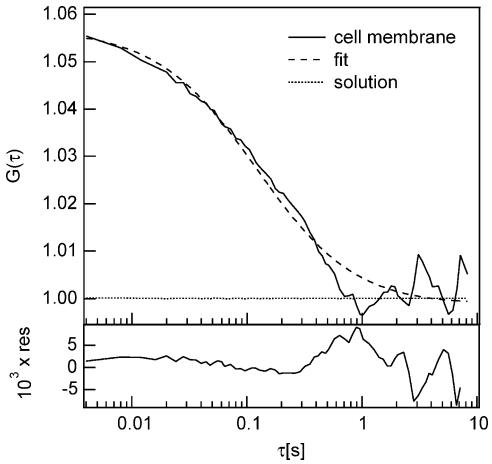

Figure 5. Decay of autocorrelation curve, $G(\tau)$, measured on the membrane of a CHO cell (continuous line) and the fit (dashed line) to eq 2. The negative control (PBS solution) did not show any correlation. Measurements were performed at 60-μW power at a wavelength of 543 nm using a P_3 pixel that has the laser focus at the center.

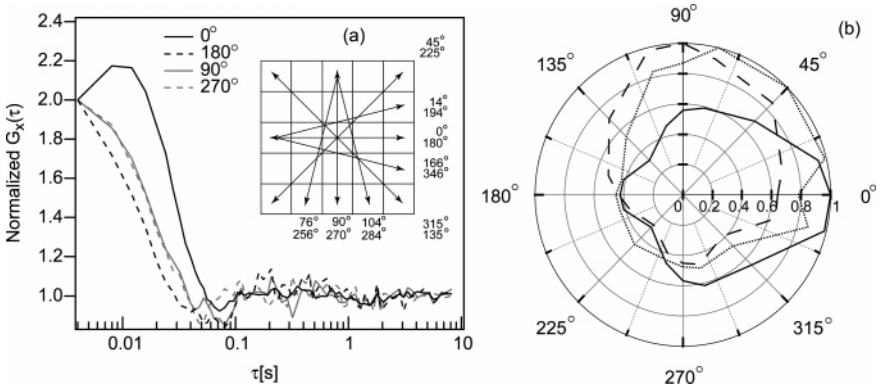

Figure 6. (a) Normalized cross-correlation function, $G_x(\tau)$, between two P_1 pixels which are 4 P_1 pixels apart calculated from the data collected on a microchannel while flowing 1 nM Atto565 in 90% glycerol at a flow rate of 30 μL/h. Inset shows the 5 × 5 array of P_1 pixels from which $G_x(\tau)$ curves for different angles were calculated. (b) Normalized width extracted from the point where the normalized $G_x(\tau)$ has a value of 1.5 and corrected for the varying distances between P_1 pixels is plotted in a polar graph.

Table 3. Flow Times τ_F and Flow Speeds for Different Flow Rates Set in the Syringe Pump[a]

	$\tau_D = 26.8 \pm 1.9$ ms	
flow rate (μL/h)	τ_F (ms)	flow speed (mm/s)
10	58.6 ± 13.7	0.0078 ± 0.0019
20	28.7 ± 5.6	0.0157 ± 0.0031
30	16.2 ± 1.8	0.0275 ± 0.0031

[a] The diffusion time τ_D deduced from no-flow data by fitting to eq 1 was used as a constant in eq 2 to fit the flow data and τ_F was obtained. Flow speed was calculated from the fucus size (0.46 μm) and τ_F.

this study and the reported values of τ_D (100 ms) on rhodamine-labeled EGFR in cultured human diploid fibroplasts.[16]

Flow Measurements. In another test, flow speeds and directions were determined in a microchannel by rotating the channel over 360° while keeping the flow rate constant. The $G(\tau)$ were calculated on the data over a region of P_3 pixel (software binned) that contains the focal spot and were fitted to the flow model (eq 3). In eq 3, τ_D was fixed to the value obtained from the "no-flow" (flow rate, 0 μL/h) data measured at a location within the microchannel at which the flow data were collected subsequently. From the obtained τ_F values and the dimension of the pinhole, the flow speed was calculated. The values of τ_D, τ_F, and the flow speed are given in Table 3 for 0° orientation of the microchannel. The flow speed was found to be proportional to the flow rate set in the syringe pump and was independent of the microchannel orientation (data not shown).

Two beam cross-correlations have been used in the past[17] to determine flow angles. Very recently it has been shown that by cross-correlating different parts of one focal volume flow direction measurements can be achieved.[18] Here it is shown that by calculating the cross-correlation $G_x(\tau)$ between pairs of P_1 pixels chosen from among the 16 P_1 pixels surrounding this P_3 area (from which the τ_F and the flow speed were determined) as shown in the inset in Figure 6a and correcting the results for varying distances between the P_1 pixels, the flow direction can be determined. The width of the $G_x(\tau)$ at half-amplitude was used as a measure of the flow time. The $G_x(\tau)$ will change depending on the flow direction. Considering two P_1 pixels A and B where flow is in the direction from A to B, forward cross-correlation A × B should give the $G_x(\tau)$ with the largest width at half-maximum while backward cross-correlation B × A against the flow should give the $G_x(\tau)$ with the shortest width at half-maximum. Cross-correlations perpendicular to the flow direction should be independent of the sequence of correlation. Experimental $G_x(\tau)$ curves (Figure 6a) show this behavior. Figure 6b shows the polar graph of normalized width determined from the point where the normalized $G_x(\tau)$ has a value of 1.5 and corrected for the varying distances between the P_1 pixels. It is clear from the polar graph that the largest width of $G_x(\tau)$ at half-maximum occurs along the direction of flow, and it changes from 0° to 45° and 90° when the microchannel was rotated from 0° to 45° and 90°. This demonstrates that flow directions can be measured in this case with a resolution of down to 14°. The angular resolution could be improved by correlating P_1 pixels with larger distances, but this would lead of course to a reduction in spatial resolution. In addition, for pixels at larger distances, the signal-to-noise ratio decreases due to the drop in the intensity when moving away from the focal spot. Thus, when a better angular resolution is needed, and the concomitant loss in spatial resolution is acceptable, the focal spot could be increased. In this work, results could be obtained up to a distance of 7 pixels leading to a spatial resolution of 2.05 μm and angular resolution of down to 9.5°.

CONCLUSION

In this work, it has been demonstrated that FCS measurements are possible using an EMCCD camera. Despite the limited time resolution, the system is well suited for the measurement of

(15) Liu, P. Department of Chemistry, National University of Singapore, 3, Science Drive 3, Singapore 117543 and Thankiah, S.; Maruyama, I.; Wohland, T. (unpublished work).

(16) Pramanik, A.; Rigler, R. *Biol. Chem.* **2001**, *382*, 371−378.

(17) (a) Brinkmeier, M.; Dörre, K.; Stephen, J.; Eigen, M. *Anal. Chem.* **1999**, *71*, 609−616. (b) Dittrich, P. S.; Schwille, P. *Anal. Chem.* **2002**, *74*, 4472−4479.

(18) Jaffiol, R.; Blancquaert, Y.; Delon, A.; Derouard, J. *Appl. Opt.* **2006**, *45*, 1225−1235.

(19) Hwang, L. C.; Leutenegger, M.; Gösch, M.; Lasser, T.; Rigler, P.; Meier, W.; Wohland, T. *Opt. Lett.* In press.

membrane proteins in living cells. It allows the multiplexing of FCS measurements, as has been demonstrated by simulations using real-time measurements on a single spot, and is capable of measuring flow speed and flow directions. With the inclusion of a dispersive element in the detection path,[4b,19] this system opens the possibility of performing spectrally resolved FCS and could thus be an important tool in the study of membrane dynamics and in the measurement of protein interactions by multicolor FCS and FCCS.

ACKNOWLEDGMENT

The authors thank Pan Xiaotao and Hanry Yu for the gift of the microchip.

Received for review January 13, 2006. Accepted March 20, 2006.

AC0600959